

Observation of gap-closing in single Josephson junctions constructed on Bi_2Te_3 surface

Yuan Pang,^{1,*} Junhua Wang,^{1,*} Zhaozheng Lyu,^{1,*} Guang Yang,¹ Jie Fan,¹
Guangtong Liu,¹ Zhongqing Ji,¹ Xiunian Jing,^{1,2} Changli Yang,^{1,2} and Li Lu^{1,2,†}

¹*Beijing National Laboratory for Condensed Matter Physics,
Institute of Physics, Chinese Academy of Sciences,
Beijing 100190, People's Republic of China*

²*Collaborative Innovation Center of Quantum Matter,
Beijing 100871, People's Republic of China*

(Dated: March 16, 2016)

Abstract

On the road of searching for Majorana fermions in condensed matter systems, a highly-sought signature is full gap-closing, as a condition for hosting the Majorana zero modes, in Josephson devices constructed on the surface of topological insulators. In this Letter, we present direct experimental evidence of gap-closing in single Josephson junctions constructed on Bi_2Te_3 surface via local contact-resistance measurement.

Recently, much attention has been paid to search for Majorana zero modes in condensed matter systems [1–4]. Majorana zero modes are expected to occur at the boundaries of p -wave-like superconductors, causing a number of peculiar phenomena. So far, a zero-bias conductance peak (ZBCP) has been observed in the conductance spectrum of interfacial junctions between p -wave-like superconductors and normal metals [5–12]. Signs of fractional Josephson effect has been observed in certain parametric region on topological insulator (TI)-based Josephson devices [13–15]. And a 4π -periodic component of current-phase relation (CPR) has been resolved in Josephson devices constructed on TI surface [16–19]. Also, dominant signals of 4π -period-like energy-phase relations (EPRs), yet being truncated to fully skewed 2π -periodic ones, have been observed on radio-frequency superconducting quantum interference devices (rf-SQUIDs) constructed on the surface of three-dimensional (3D) TI Bi_2Te_3 [20].

For Josephson junctions constructed on TI surface, the full transmission and perfect Andreev reflection of helical electrons lead to the formation of two branches of 4π -periodic EPRs [21–27]. These two branches have opposite parities, and evolve oppositely with the variation of the phase difference across the junction. The energy separation between the two branches defines the minigap of the junction. At π phase difference, the two branches cross with each other at the fermi energy, so that the minigap is closed and the Majorana zero modes are expected [28–32]. Recently, we have employed the rf-SQUID structure to realize the π phase difference by threading half flux quantum into the ring of the rf-SQUID, and observed fully skewed EPRs truncated from 4π -periodic trends [20]. Along this direction, however, what is missing is the verification of the same scenario directly on single Josephson junctions, based on which the idea was firstly proposed [29] and further details were discussed [32].

In this Letter, we report investigations, through local contact resistance measurement, on the evolution of the minigap in single Josephson junctions constructed on the surface of Bi_2Te_3 . Our results reflect the existence of topologically-protected gap-closing and perfect transmission of quasiparticle transport in the junctions, which are in line with the scenario that Majorana zero modes could be hosted in this type of devices.

The $\text{Pb-Bi}_2\text{Te}_3\text{-Pb}$ single Josephson junctions were fabricated on exfoliated Bi_2Te_3 flakes of ~ 100 nm in thickness, with normal-metal Pd electrodes attached to different places in the junction area to detect the local minigap. An over-exposed poly(methyl methacrylate)

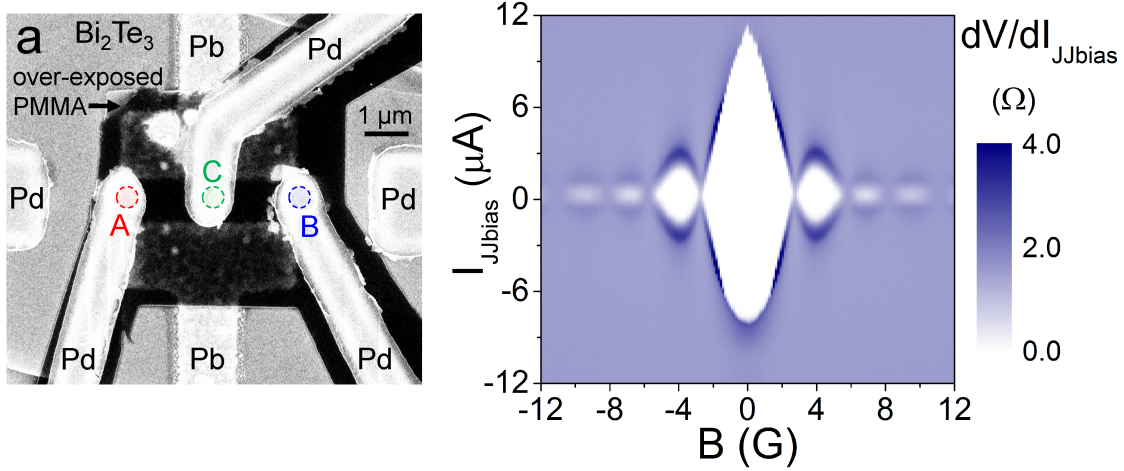


FIG. 1: (color online) (a) SEM image of a typical device. It contains two “T”-like Pb electrodes deposited on top of a Bi_2Te_3 flake, forming a Josephson junction via superconducting proximity effect at low temperatures. Three additional Pd electrodes are attached to the Bi_2Te_3 surface in the junction area at positions A, B and C marked by the dashed red, blue and green circles, respectively, with the help of an insulating mask of over-exposed PMMA layer (in black) to prevent the rest part of the Pd electrodes to contact with the Pb and Bi_2Te_3 . (b) The Fraunhofer diffraction pattern of the Josephson junction measured at $T \approx 20$ mK. The white area represents the zero-resistance state.

(PMMA) layer with windows of ~ 600 nm in diameter was used to isolate the rest of the Pd electrodes from touching the flake and the Pb films. Figure 1(a) shows the scanning electron microscope (SEM) image of a typical device with Pd electrodes A, B and C located at the left side, the right side and the center of the junction, with the contacting points marked with red, blue and green dashed circles, respectively. The contact resistance of these electrodes was measured by using a three-terminal measurement configuration [33] and lock-in amplifier technique, down to a low temperature of ~ 20 mK in a dilution refrigerator.

Before presenting the results of the contact resistance, let us first show in Fig. 1(b) the differential resistance $dV/dI_{JJ\text{bias}}$ of the Pb- Bi_2Te_3 -Pb Josephson junction, which was measured between the two Pb electrodes as a function of magnetic field B and bias current $I_{JJ\text{bias}}$ at the base temperature of $T \approx 20$ mK. The white-colored area represents the zero-resistance state. Standard Fraunhofer diffraction pattern was obtained. The slight asymmetry of the pattern between positive and negative directions of $I_{JJ\text{bias}}$ is caused by

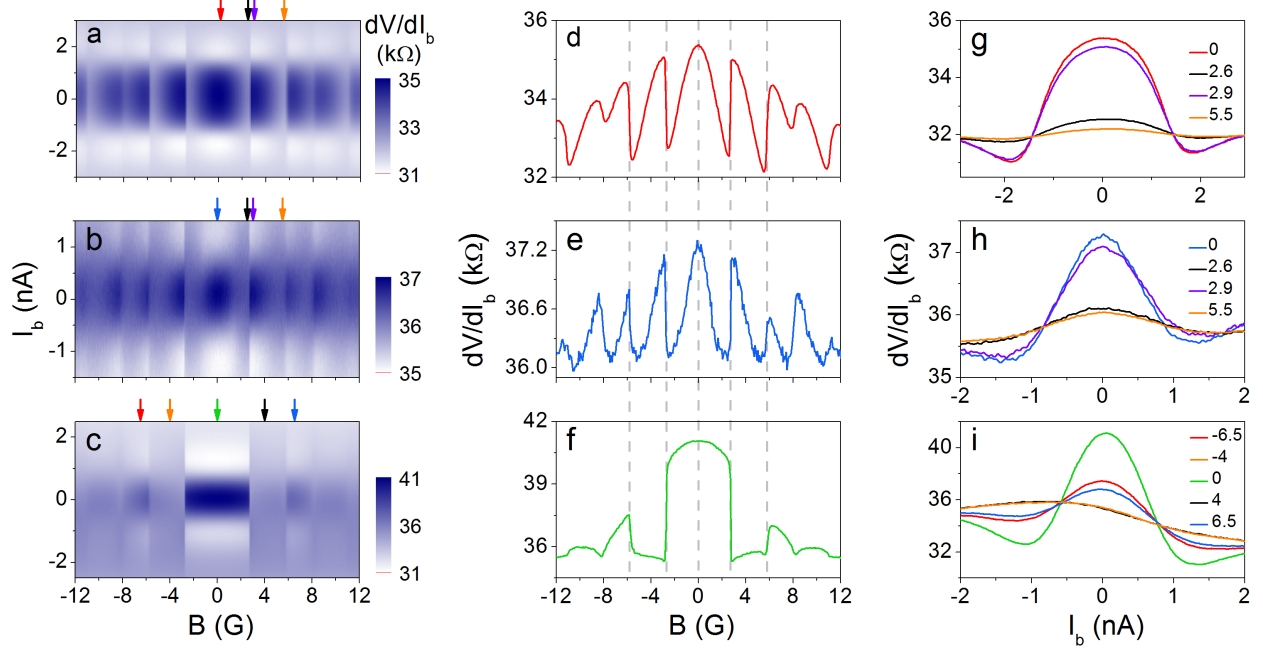


FIG. 2: (color online) (a), (b) and (c) The 2D plots of contact resistance dV/dI_b at position A, B and C, respectively, as a function of magnetic field and bias current, at $T \approx 20$ mK. (d), (e) and (f) The horizontal line cuts of dV/dI_b at $I_b = 0$ in (a), (b) and (c), respectively. (g), (h) and (i) The vertical line cuts of dV/dI_b in (a), (b) and (c), respectively, at positions indicated by the arrows of the same color in the corresponding 2D plots. The numbers in the legends are in the unit of Gauss.

the hysteresis of $I_{JJ\text{bias}} - V$ characteristics, which is frequently seen in TI-based Josephson junctions. The period of the Fraunhofer pattern is $\Delta B = 2.8 \pm 0.2$ G. It corresponds to an effective area of $S_{\text{eff}} = \phi_0/\Delta B = 7.14 \mu\text{m}^2$ (where $\phi_0 = h/2e$ is flux quantum, e is the electron charge, and h is the Planck constant). This estimated S_{eff} is in good agreement with $4\mu\text{m} \times 1.8\mu\text{m} = 7.2 \mu\text{m}^2$, the geometric area of the junction after considering flux compression [34].

Shown in Figs. 2(a), 2(b) and 2(c) are the 2D color plots of the contact resistance dV/dI_b measured at positions A, B and C, respectively, as a function of B and bias current I_b . The dV/dI_b shows a peak around zero bias current/voltage (Figs. 2(g), 2(h) and 2(i)). As will be explained later, this peak structure correlates to the local minigap in Bi_2Te_3 .

The most peculiar feature in Fig. 2 is the abrupt jumps in dV/dI_b , which happens simultaneously at positions A, B and C, when the flux reaches the nodes of the Fraunhofer

pattern. Despite that the peaks in the Fraunhofer pattern are sinusoidal-like, the dV/dI_b at positions A and B shows a skewed flux dependence followed by abrupt jumps, i.e., the minigap gradually changes from its most pronounced state at zero flux to the gap-closing state as the flux is ramped to the nodes of the Fraunhofer pattern, then suddenly jumps to the pronounced state again as passing the nodes. The skewed behavior can be more clearly seen from the horizontal line cuts of the 2D plots at $I_b = 0$, which are shown in Figs. 2(d) and 2(e).

The flux-dependent evolution of minigap can also be clearly seen from the vertical line cuts of the 2D plots. The black and orange curves shown in Figs. 2(g) and 2(h) are the vertical line cuts taken from the corresponding 2D plots at $B = 2.6$ G and 5.5 G, respectively. The minigap on these curves is largely suppressed. In the supplementary materials, we will present more evidence of gap-closing observed on additional device [34]. We note, as will be shown later, that the remaining shape of the gap in Figs. 2(g) and 2(h) is presumably caused by the finite size effect of the Pd contact, as well as their misalignment to the ends of the junction.

Also very unusual is the flux dependence of the minigap at position C, where abrupt jumps between gap-opening and gap-closing states were observed (Figs. 2(c), 2(f) and 2(i)). From Fig. 2(c), the minigap can be clearly resolved in the flux ranges of even numbered Fraunhofer peaks, whereas it disappears in the flux range of the first Fraunhofer peak. Such an even-odd behavior would hint that each jump is accompanied by a π phase shift.

The fact that the dV/dI_b and the Fraunhofer pattern share the same oscillation periods reflects that the dV/dI_b is correlated to the CPR/EPR of the junction. For a proximity-effect-type of S-N-S Josephson junction, it is known that the energies of the Andreev bound states in the junction, thus the minigap in Bi_2Te_3 , shall oscillate with the flux [29]. Since the contact resistance in this experiment is higher than the quantum unit $h/2e^2 = 12.9\text{k}\Omega$, the measurement was in the tunneling regime, revealing mostly the information of the electron density of states in Bi_2Te_3 . Therefore, we believe that the oscillation of dV/dI_b is caused by the oscillation of the minigap in Bi_2Te_3 , and that the dV/dI_b peak is a reflection of the minigap.

The minigap can be calculated as follows. Firstly, in the absence of I_{JJbias} , the local phase

difference across the junction can be expressed as:

$$\varphi(B, x) = 2\pi \frac{BHx}{\phi_0} \pm \pi \text{int}\left(\frac{\phi}{\phi_0}\right) \quad (1)$$

where x is defined from $-W/2$ to $W/2$, W is the width of the junction, H is the effective distance between the two Pb electrodes of the junction after considering flux compression [34], and ϕ is the total flux in the junction. The first term in Eq. 1 is the phase difference caused by magnetic flux. The second term represents a π phase jump whenever the flux in the junction is varied across the nodes of the Fraunhofer pattern.

For the mechanism of the π phase jump, it is known that the phase difference constant, θ , in a single Josephson junction can be self-adjusted according to the criteria of minimizing the total energy. As can be seen in the supplementary materials [34], in the flux range of the 0th Fraunhofer peak, the lowest-energy state corresponds to the $\theta = 0$ state, but in the flux range of the 1st Fraunhofer peak, the lowest-energy state corresponds to the $\theta = \pm\pi$ state. A π phase shift will thus take place at the nodes of the Fraunhofer pattern.

The minigap is the energy separation between the two lowest-energy branches of Andreev bound states whose EPRs are [35–37]: $E_n = \pm\Delta_0[1 - D_n \sin^2(\varphi/2)]^{1/2}$ (where E_n and D_n are the energy and the transmission coefficient of the n^{th} allowed mode of the quasiparticles, respectively). It can be seen that only in the fully transparent limit (i.e., $D_n = 1$ for all modes) can the minigap be fully closed, and thus the observed gap-closing phenomenon be interpreted. In this limit, the minigap can be simplified as:

$$\Delta \propto |\cos(\varphi/2)| \quad (2)$$

The minigap will be obviously open even if the transmission coefficient is as high as 0.99, as illustrated in the supplementary materials [34] and demonstrated experimentally in a Josephson junction using a single atomic layer of graphene as the barrier [38]. For the Pb-Bi₂Te₃-Pb junctions in this experiment, which contain two Pb-Bi₂Te₃ interfaces and a Bi₂Te₃ part of 1 μm in length, the total transmission coefficient is expected to be much less than 1 if without a mechanism to protect the full transparency. The observed full gap-closing, therefore, reflects the existence of topologically-protected full transparency of quasiparticle transport in our devices. This is actually expected on the TI surface where the helical states are topologically protected from backscattering, resulting in perfect Andreev reflections and the gap-closing. We note that it is these surface states that are most likely detected in our contact resistance measurement, despite the existence of the bulk states in Bi₂Te₃.

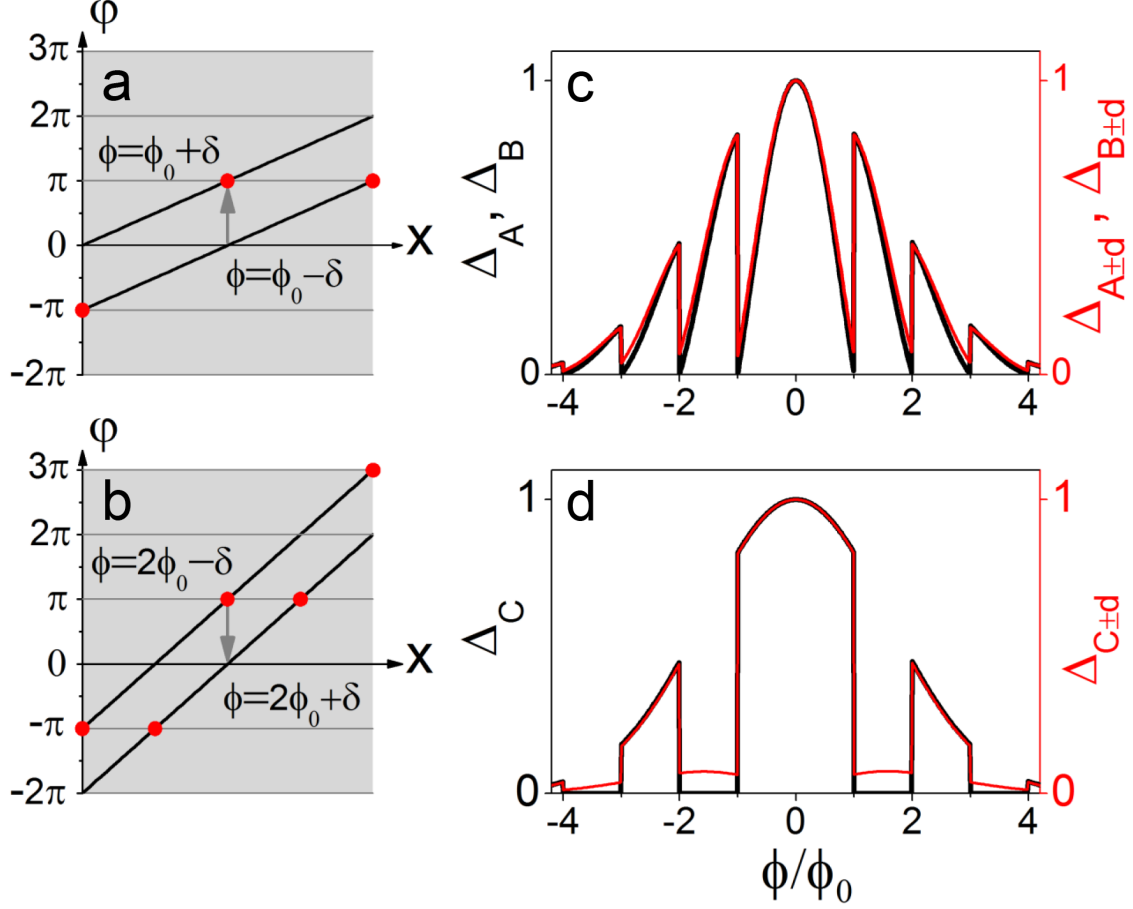


FIG. 3: (color online) (a) and (b) The local phase difference of the junction as a function of position x at flux of ϕ_0 and $2\phi_0$, respectively. The left edge of the plots corresponds to $x = -W/2$ and the right edge to $x = W/2$. The phase distribution line undergoes a global π phase shift at these flux, as indicated by the gray arrows. The red circles highlight the positions where a π phase difference is reached, therefore the local minigap is closed. (c) The calculated minigap Δ at $x = \pm W/2$ (black) and $x = \pm W/2 \pm 100$ nm (red). (d) The calculated Δ at $x = 0$ (black) and ± 100 nm (red).

In a control experiment on similar devices constructed on topologically-trivial metal (Au film) instead of Bi_2Te_3 [34], we show that, without protected full transparency, the minigap will not be fully closed with varying magnetic flux, resulting in only a faint and jumpless oscillatory pattern of dV/dI_b .

With Eqs. 1 and 2, the local minigap can be calculated. Figures 3(a) and 3(b) show the phase distribution line across the junction near the first and the second Fraunhofer nodes, respectively. This line changes its slope with varying magnetic flux, rotating about the center

of the junction. The red circles represent where $\varphi(x)$ reaches odd multiples of π , so that the local minigap is closed and Majorana zero mode is presumably hosted [32]. The positions of the red circles located near the ends of the junction move with the rotation of the phase distribution line, so that a skewed pattern of dV/dI_b is detected at positions A and B (Figs. 2(d) and 2(e)). When the flux is varied across the Fraunhofer nodes, a π phase jump occurs (indicated by the gray arrows). The positions of gap-closing jump accordingly. At position C, the center of the junction, however, the dV/dI_b behaves differently. It seems that the minigap either keeps opening within the flux ranges of the even numbered Fraunhofer peaks, or keeps closing within the flux ranges of the 1st Fraunhofer peaks. In the latter range the gap-closing point is pinned at the center of the junction while the phase distribution line rotates about the center of the junction with varying flux.

Shown in Figs. 3(c) and 3(d) are the calculated minigap at positions A/B and C, respectively. The black curves represent the minigap strictly at positions A/B or C, and the red curves represent the minigap at positions that deviate from that of the black curves by an amount of $d = \pm 100$ nm. Since the overall amplitude of the minigap decays rapidly in magnetic field, we have phenomenologically imposed a Gaussian-like envelope $e^{-\gamma(\phi/\phi_0)^2}$ (where $\gamma = 0.2$ is a fitting parameter) to the minigap shown in Figs. 3(c) and 3(d), in order to compare with the experimental data.

From the difference between the black and the red curves in Figs. 3(c) and 3(d), it can be seen that the gap-closing point is very sensitive to x . However, the position of gap-closing will be thermally smeared, having an uncertainty of ~ 200 nm at the measurement temperature of ~ 20 mK [20]. On the other hand, the alignment accuracy of the Pd electrodes in our experiment is around $d = \pm 100$ nm. The nominal contact area of the Pd electrodes has a diameter of 600 nm (the effective contacting area might be smaller). Due to these factors, it is natural that there will be some tiny feature of gap remaining on the black and orange curves in Figs. 2(g) and 2(h). We believe that within the accuracy of this experiment we have already observed gap-closing.

To further test our model, we have measured the dV/dI_b as a function of B and $I_{JJ\text{bias}}$ at $I_b = 0$. The data obtained at positions A and B are presented in Figs. 4(a) and 4(b), respectively. These data are compared with the calculated minigap shown in Figs. 4(c) and 4(d), respectively. Good agreements were obtained.

It is known that the phase distribution line in Figs. 3(a) and 3(b) can be shifted upwards

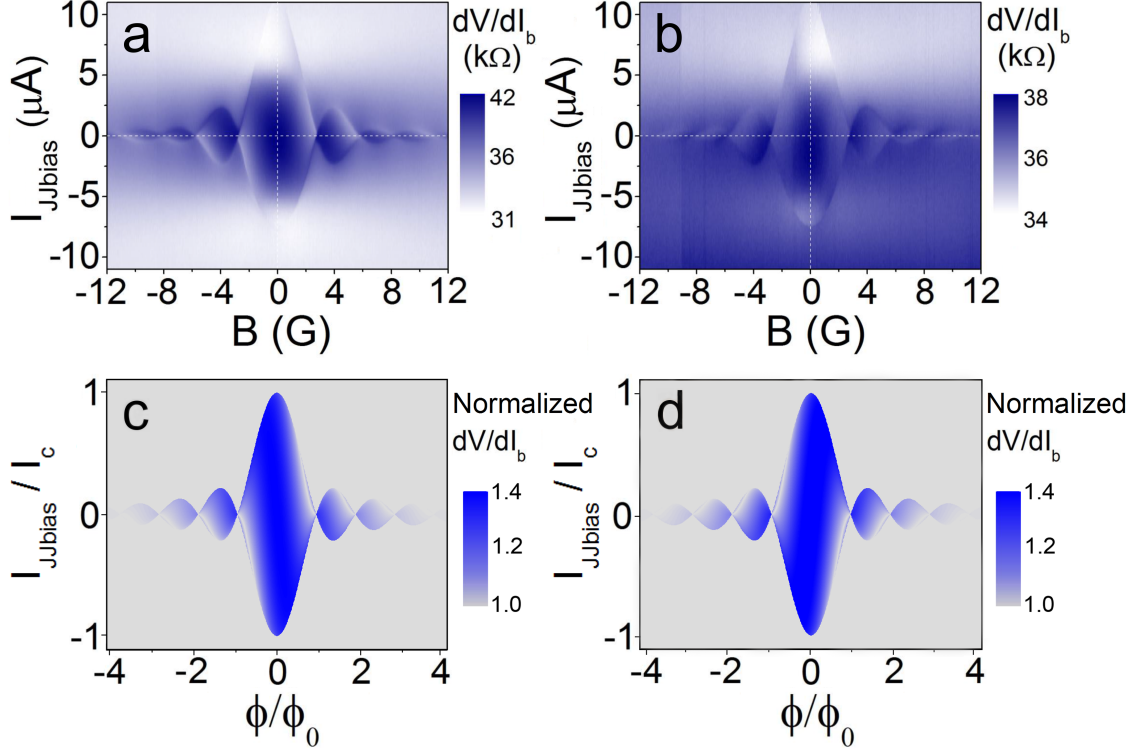


FIG. 4: (color online) (a) and (b) Contact resistance measured at positions A and B, respectively, as a function of magnetic field and I_{JJbias} , the bias current to the Pb-Bi₂Te₃-Pb Josephson junction, at $T \approx 20$ mK. During the measurements the dc bias current to the Pd contacts was set to zero ($I_b = 0$), and the ac excitation current was 0.5 nA. (c) and (d) The calculated dV/dI_b at positions A and B, respectively, as a function of normalized flux and normalized I_{JJbias} in arbitrary units of color scale.

or downwards by I_{JJbias} , in addition to being rotated by magnetic flux. In the presence of I_{JJbias} and thus the upwards or downwards shift, the distribution of local supercurrent density is no longer symmetrical at the center of the junction ($x = 0$). This makes the dV/dI_b at position A and B to behave differently, so that their 2D plots become distinguishable.

The additional phase shift caused by I_{JJbias} can be estimated via the Josephson equation [39]: $I_s = I'_c \sin \varphi$, where I_s is the total supercurrent, $I'_c = I_c |\frac{\sin(\pi\phi/\phi_0)}{\pi\phi/\pi_0}|$ is the Fraunhofer envelope, and I_c is the total critical supercurrent of the junction at zero field. With this additional phase shift, Eq. 1 can be rewritten as:

$$\varphi(B, x) = 2\pi \frac{BHx}{\phi_0} \pm \pi \text{int}\left(\frac{\phi}{\phi_0}\right) + \arcsin\left(\frac{I_{JJbias}}{I_c} \left| \frac{\pi\phi/\phi_0}{\sin(\pi\phi/\phi_0)} \right| \right) \quad (3)$$

It can be proven that the flux at which the π phase jump happens does not change with

I_{JJbias} , as has been assumed in Eq. 3. The minigap Δ in the presence of I_{JJbias} can be calculated by using Eqs. 2 and 3. And the dV/dI_b can further be mapped via the relation $dV/dI_b \propto e^{\Delta/k_B T}$, where $\Delta/k_B T = 0.5e^{-0.2(\phi/\phi_0)^2} |\cos(\varphi/2)|$ has been assumed. The results are shown in Figs. 4(c) and 4(d), mimicking reasonably well the experimental data.

To summarize, we have performed contact resistance measurement on single Josephson junctions constructed on Bi_2Te_3 surface. The observed behavior of full gap-closing at ultralow temperatures can only be interpreted within a scenario when the quasiparticle transport is fully transparent in the devices. Our results are consistent with the theoretical predictions that Majorana zero modes can be formed in S-TI-S type of Josephson junctions.

Acknowledgments We would like to thank L. Fu, Z. Fang, X. Dai, T. Xiang, X. C. Xie, Q. F. Sun, R. Du, G. M. Zhang and X. Hu for fruitful discussions. This work was supported by the National Basic Research Program of China from the MOST under the grant No. 2009CB929101 and 2011CB921702, by the NSFC under grant No. 91221203, 11174340, 11174357, 91421303 and 11527806, and by the Strategic Priority Research Program B of the Chinese Academy of Sciences under the grant No. XDB07010100.

* These authors contribute equally to this work.

† Corresponding authors: lilu@iphy.ac.cn

- [1] E. Majorana, *Nuovo Cimento* **14**, 171-184 (1937).
- [2] F. Wilczek, *Nature Phys.* **5**, 614-618 (2009).
- [3] R. F. Service, *Science* **332**, 193-195 (2011).
- [4] M. Franz, *Physics* **3**, 24 (2010); M. Franz, arXiv: 1302.3641v1.
- [5] V. Mourik, K. Zuo, S. M. Frolov, S. R. Plissard, E. P. A. M. Bakkers, and L. P. Kouwenhoven, *Science* **336**, 1003-1007 (2012).
- [6] M. T. Deng, C. L. Yu, G. Y. Huang, M. Larsson, P. Caroff, and H. Q. Xu, *Nano Lett.* **12**, 6414-6419 (2012).
- [7] A. Das, Y. Ronen, Y. Most, Y. Oreg, M. Herblum, and H. Shtrikman, *Nature Phys.* **8**, 887-895 (2012).
- [8] H. O. H. Churchill, V. Fatemi, K. Grove-Rasmussen, M. T. Deng, P. Caroff, H. Q. Xu, and

- C. M. Marcus, Phys. Rev. B **87**, 241401 (2013).
- [9] A. D. K. Finck, D. J. Van Harlingen, P. K. Mohseni, K. Jung, and X. Li, Phys. Rev. Lett. **110**, 126406 (2013).
 - [10] S. Nadj-Perge, I. K. Drozdov, J. Li, H. Chen, S. Jeon, J. Seo, A. H. MacDonald, B. A. Bernevig, and A. Yazdani, Science **346**, 602-607 (2014).
 - [11] S. Sasaki, M. Kriener, K. Segawa, K. Yada, Y. Tanaka, M. Sato, and Y. Ando, Phys. Rev. Lett. **107**, 217001 (2011).
 - [12] F. Yang, Y. Ding, F. Qu, J. Shen, J. Chen, Z. Wei, Z. Ji, G. Liu, J. Fan, C. Yang, T. Xiang, and L. Lu, Phys. Rev. B **85**, 104508 (2012).
 - [13] L. P. Rokhinson, X. Liu, and J. K. Furdyna, Nature Phys. **8**, 795-799 (2012).
 - [14] V. S. Pribiag, A. J. Beukman, F. Qu, M. C. Cassidy, C. Charpentier, W. Wegscheider, and L. P. Kouwenhoven, Nature Nanotechnology **10**, 593-597 (2015).
 - [15] J. Wiedenmann, E. Bocquillon, R. S. Deacon, S. Hartinger, O. Herrmann, T. M. Klapwijk, L. Maier, C. Ames, C. Brüne, C. Gould, A. Oiwa, K. Ishibashi, S. Tarucha, H. Buhmann, and L. W. Molenkamp, Nature Commun. **7**, 10303 (2016).
 - [16] C. Kurter, A. D. K. Finck, P. Ghaemi, Y. S. Hor, and D. J. Van Harlingen, Phys. Rev. B **90**, 014501 (2014).
 - [17] S. P. Lee, K. Michaeli, J. Alicea, and A. Yacoby, Phys. Rev. Lett. **113**, 197001 (2014).
 - [18] I. Sochnikov, L. Maier, C. A. Watson, J. R. Kirtley, C. Gould, G. Tkachov, E. M. Hankiewicz, C. Brüne, H. Buhmann, L. W. Molenkamp, and K. A. Moler, Phys. Rev. Lett. **114**, 066801 (2015).
 - [19] C. Kurter, A. D. K. Finck, Y. S. Hor, and D. J. Van Harlingen, Nature Commun. **6**, 7130 (2015).
 - [20] Y. Pang, J. Shen, F. Qu, Z. Lyu, J. Wang, J. Feng, J. Fan, G. Liu, Z. Ji, X. Jing, C. Yang, Q. Sun, X. C. Xie, L. Fu, and L. Lu, arXiv:1503.00838v2.
 - [21] A. Yu Kitaev, Phys.-Usp. **44**, 131 (2001).
 - [22] H. J. Kwon, V. M. Yakovenko, and K. Sengupta, Low Temp. Phys. **30**, 613 (2004).
 - [23] L. Fu and C. L. Kane, Phys. Rev. B **79**, 161408 (2009).
 - [24] R. M. Lutchyn, J. D. Sau, and S. Das Sarma, Phys. Rev. Lett. **105**, 077001 (2010).
 - [25] M. Diez, I. C. Fulga, D. I. Pikulin, M. Wimmer, A. R. Akhmerov, and C. W. J. Beenakker, Phys. Rev. B **87**, 125406 (2013).

- [26] B. J. Wieder, F. Zhang, and C. L. Kane, Phys. Rev. B **89**, 075106 (2014).
- [27] C. W. J. Beenakker, D. I. Pikulin, T. Hyart, H. Schomerus, and J. P. Dahlhaus, Phys. Rev. Lett. **110**, 017003 (2013).
- [28] N. Read and D. Green, Phys. Rev. B **61**, 10267 (2000).
- [29] L. Fu and C. L. Kane, Phys. Rev. Lett. **100**, 096407 (2008).
- [30] Y. Oreg, G. Refael, and F. von Oppen, Phys. Rev. Lett. **105**, 177002 (2010).
- [31] T. D. Stanescu, R. M. Lutchyn, and S. Das Sarma, Phys. Rev. B **84**, 144522 (2011).
- [32] A. C. Potter and L. Fu, Phys. Rev. B **88**, 121109 (2013).
- [33] We note that when the contact resistance is much larger than the sample resistance, which is the case in this experiment, the signal obtained in a three-terminal measurement configuration is dominated by the contact resistance of the electrode that shared by the current loop and the voltage loop.
- [34] See Supplemental Material at [URL will be inserted by publisher] for more data and discussions.
- [35] C. W. J. Beenakker, *Transport phenomena in Mesoscopic Systems*, H. Fukuyama and T. Ando, eds. Springer, Berlin (1992).
- [36] T. M. Klapwijk, *Journal of Superconductivity: Incorporating Novel Magnetism* **17**, 593 (2004).
- [37] A. A. Golubov, M. Y. Kupriyanov, and E. Il'ichev, Rev. Mod. Phys. **76**, 411 (2004).
- [38] G. H. Lee, S. Kim, S. H. Jhi, and H. J. Lee, Nature Commun. **6**, 6181 (2015).
- [39] A. Barone, *Physics and Application of the Josephson Effect*. John Wiley and Sons, Inc. (1982).

Supplementary Materials for
“Observation of gap-closing on single Josephson junctions constructed
on Bi₂Te₃ surface”

Yuan Pang^{1,*}, Junhua Wang^{1,*}, Zhaozheng Lyu^{1,*}, Guang Yang¹, Jie Fan¹, Guangtong Liu¹,
Zhongqing Ji¹, Xiunian Jing^{1,2}, Changli Yang^{1,2} and Li Lu^{1,2†}

*1 Beijing National Laboratory for Condensed Matter Physics, Institute of Physics,
Chinese Academy of Sciences, Beijing 100190, People's Republic of China*

2 Collaborative Innovation Center of Quantum Matter, Beijing 100871, People's Republic of China

* These authors contributed equally to this work.

† Corresponding authors: lilu@iphy.ac.cn

Contents:

1. Contact resistance obtained on another device with three Pd electrodes
2. Control experiment on Pb-Au-Pb Josephson devices
3. The mechanism of π phase shift in a single Josephson junction
4. The minigap in S-N-S Josephson junctions with different transparency to quasiparticle process
5. Estimation of effective junction area after considering flux compression

1. Contact resistance obtained on another device with three Pd electrodes

We have fabricated several devices with three contact positions in the junction area. Figure S1a shows the SEM image of one such device (named by device #S1). Figure S1b shows the differential resistance of contact position B and C. The blue curve (position B) shows a skewed oscillation against magnetic field, and the green curve (position C) shows an on/off-like oscillation. And all the curves are accompanied with abrupt jumps whenever flux passes the Fraunhofer nodes, in agreement with the data shown in the main manuscript.

Shown in Fig. S1c and d are the color plots of contact resistance measured at positions C and B, respectively, as functions of magnetic field and bias current. And shown in Fig. S1e and f are the line cuts of Fig. S1c and d respectively, as a function of bias current injected from the contact position. The results are similar to the ones presented in the main manuscript.

From Fig. S1e and f we can see that the red/pink curve shows clearly an enhanced resistance peak (a superconducting mini-gap structure), whereas the black/orange curve is gapless.

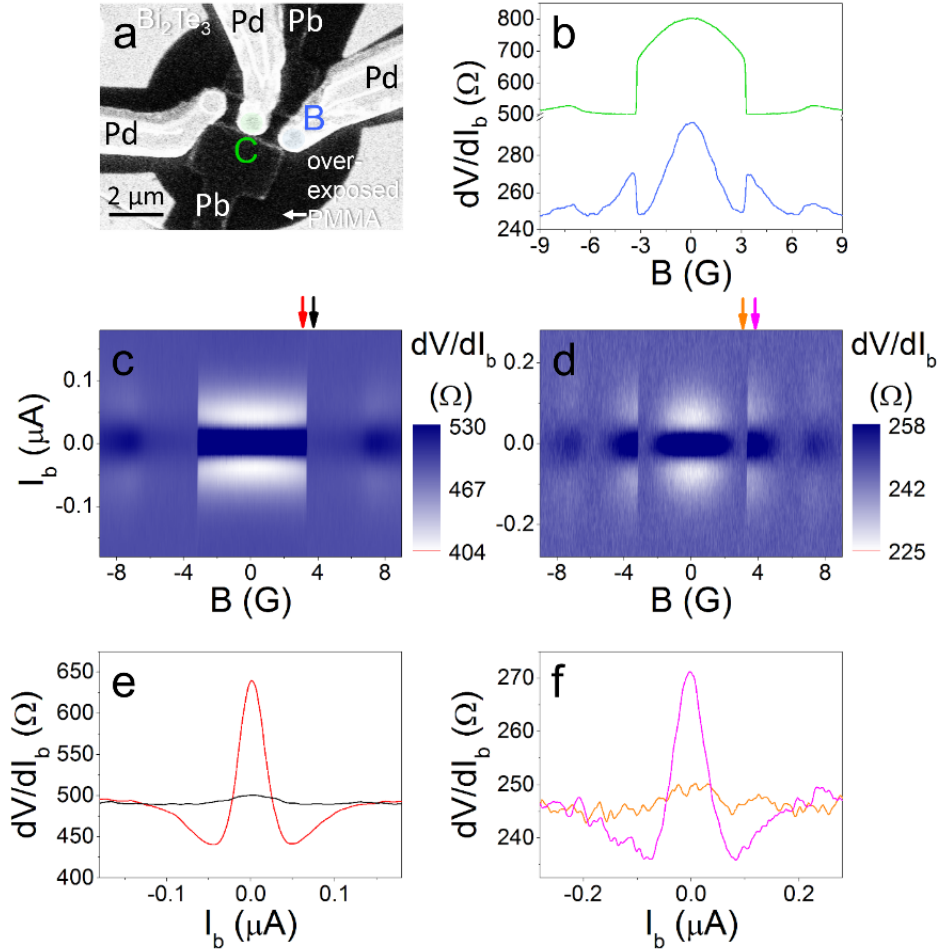


FIG. S1 | (a) SEM image of device #S1. (b) Differential resistance of position C (green curve) and B (blue curve), respectively, as a function of magnetic field. (c), (d) Color plots of contact resistance measured at positions C and B, respectively, as functions of magnetic field and bias current. (e) The differential resistance curves of position C as a function of bias current before/after jumping. The colored curves are line cuts at the fields marked by the arrows of the same color in Fig. S1c. (f) The differential resistance curves of position B as a function of bias current before/after jumping. The colored curves are line cuts at the fields marked by the arrows of the same color in Fig. S1d. All the measurements were performed at ~ 20 mK.

2. Control experiment on Pb-Au-Pb Josephson devices

We have fabricated several Pb-Au-Pb proximity-effect Josephson junctions, each with two point contact-like Pd electrodes to the two ends of the junction area on Au film, and performed transport measurements down to ~ 20 mK or 200 mK. The results are similar. In the following we present the results obtained on one of such devices measured at 200 mK. The SEM picture of the device is shown in Fig. S2a. The supercurrent of this device demonstrates a standard Fraunhofer pattern for small Josephson junctions, as shown in Fig. S2b, with a critical supercurrent of up to ~ 100 μ A. Figures S2c and S2d show the contact resistance dV/dI_b of the Pd electrodes at the upper and lower ends of the junction, respectively. Un-skewed sinusoidal patterns are obtained, with no sign of jumps. Figures S2e and S2f show the line cuts in Figs. S2c and S2d at $I_b=0$, respectively. No oscillatory structure can be resolved within the resolution limit, indicating that the gap is never closed at zero bias.

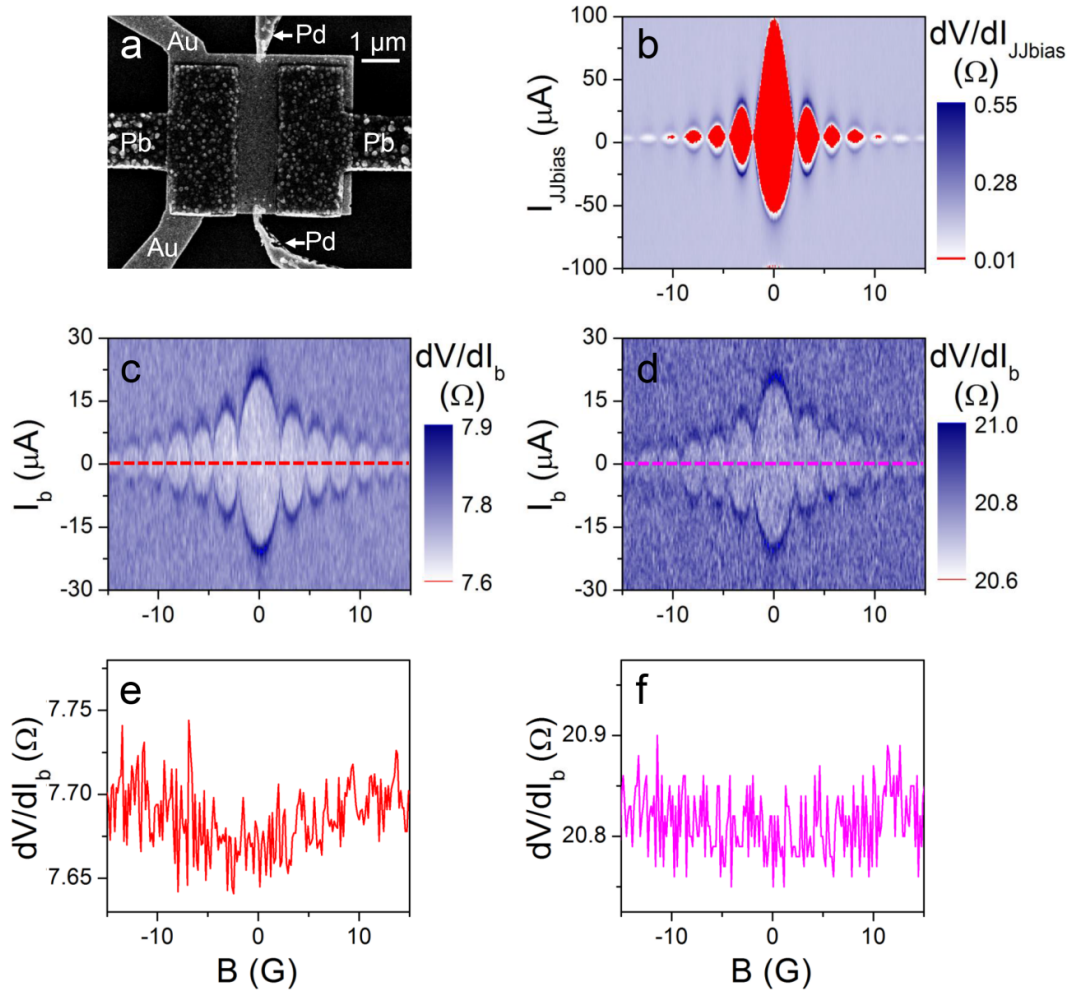


FIG. S2 | (a) SEM image of the Pb-Au-Pb device, with two point contact-like Pd electrodes connecting to the two ends of the junction. (b) Fraunhofer diffraction pattern of the Pb-Au-Pb Josephson junction, as functions of magnetic field B and current $I_{JJ,bias}$ flowing through the junction. The red colored area represents the zero-resistance state. (c) and (d) The measured contact resistance by the Pd electrodes at the upper and lower ends of the junction, respectively, as functions of magnetic field and the bias current injected into each contact. (e) and (f) the line cuts (c) and (d) at $I_b=0$, respectively. The transport measurements were performed at ~ 200 mK.

The dV/dI_b of Au-Pd point contacts has a low-resistance state near the zero bias. There the conductance enhancement is caused by Andreev reflection at the S-N interface, and can be explained within the BTK theory (G. E. Blonder, M. Tinkham, M. T. Klapwijk, Phys. Rev. B 25, 4515 (1982)). The envelope of the low-resistance state in Figs. S2c and S2d is related to a characteristic critical current, which is not but the local excess current of the S-N interface: $I_e \propto (\Delta/eR) \tanh(V/2k_B T)$, where R is the normal-state resistance of the point contact, and Δ is the local minigap in superconducting Au (see A. Barone, *Physics and application of the Josephson effect*. John Wiley and Sons, Inc. 1982). In the large- V limit, the shape of the envelope is determined by Δ .

The shape of the low-resistance state in Figs. S2c and S2d is similar to the Fraunhofer pattern shown in Fig. S2b. However, it has to be pointed out that the measured pattern by each Pd contact only probes the local S-N-like transition with increasing I_b , not the Fraunhofer pattern which is a globally integrated feature. This conclusion is reasonable because the bias current used in the contact resistance measurements is significantly smaller than the total critical supercurrent of the Pb-Au-Pb junction.

3. The mechanism of π phase shift in a single Josephson junction

In the following we will show that near the node fields of the Fraunhofer pattern the phase constant of a single Josephson junction can be freely adjusted between 0 and π , both states have the same total energy and carry zero net current. The total energy of the two states is:

$$E_J = \begin{cases} \frac{\Delta_0}{W} \int_{-\frac{W}{2}}^{\frac{W}{2}} [1 - \cos(\frac{2\pi\phi}{\phi_0})] dx & (\text{without } \pi \text{ phase shift}) \\ \frac{\Delta_0}{W} \int_{-\frac{W}{2}}^{\frac{W}{2}} [1 - \cos(\frac{2\pi\phi}{\phi_0} \pm \pi)] dx & (\text{with } \pi \text{ phase shift}) \end{cases}$$

$$= \begin{cases} \Delta_0 [1 - \frac{\sin(\pi\phi/\phi_0)}{\pi\phi/\phi_0}] & (\text{without } \pi \text{ phase shift}) \\ \Delta_0 [1 + \frac{\sin(\pi\phi/\phi_0)}{\pi\phi/\phi_0}] & (\text{with } \pi \text{ phase shift}) \end{cases}$$

where Δ_0 is a constant, $\phi=BHx$ is the flux in the junction area, H is the effective length and W the width of the junction.

Shown in Fig. S3 is the calculated E_J of the two states with (red) and without (blue) the π phase shift. In order for the system to trace the lowest energy state, a π phase shift will happen at the node fields of the Fraunhofer pattern, accompanied with the reverse of the screening supercurrent against the Josephson vortex.

It should be noted that the π phase shift in a single Josephson junction as discussed above is different from the π phase shift in a rf-SQUID constructed on the surface of TI (Y. Pang et.al., arXiv:1503.00838v2). In the rf-SQUID structure, there is no adjustable phase different constant, since the two superconducting pads are connected by the superconducting ring. The π phase shift observed there could only be attributed to a topologically nontrivial mechanism – quasiparticle-poisoning-mediated inter-branch switching between two 4π -periodic EPRs with opposite parities.

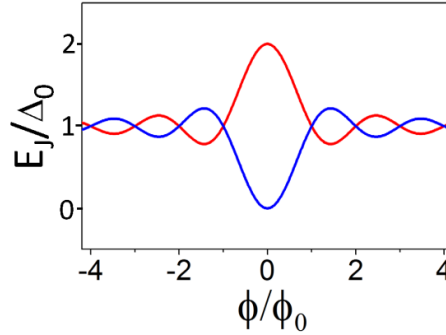


FIG. S3 | Two branches of energy-flux relation of the Josephson junction.

4. The minigap in S-N-S Josephson junctions with different transparency to quasiparticle process

The minigap is the energy separation between the two lowest-energy branches of Andreev bound states whose EPRs are:

$$E_n = \pm \Delta_0 [1 - D_n \sin^2(\phi/2)]^{1/2}$$

where E_n and D_n are the Josephson energy and the transmission coefficient of the n^{th} allowed mode of the quasiparticles in the junction, respectively. The curves plotted in Fig. S4 are the calculated E_n at several different D_n . It can be seen that the minigap is significantly not fully closed even if the transmission coefficient is as high as 0.99. Full gap closing only happens when $D_n=1$.

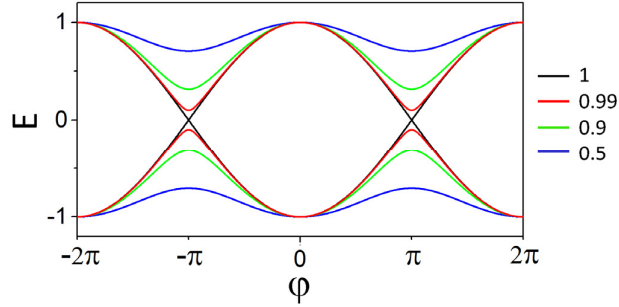


FIG. S4 | The energy-phase relation of the lowest-energy Andreev bound states at several different transmission coefficient.

5. Estimation of the effective junction area after considering flux compression

In Fig. S5 we illustrate how the effective junction area of the device shown in Fig. 1 of the main manuscript is calculated after considering flux compression and stray supercurrent distribution.

As illustrated in the upper left panel of Fig. S5, below H_{c1} the magnetic field cannot penetrate into the bulk of superconducting Pb film other than within the penetration depth. The flux lines will therefore be pushed away from the Pb electrodes and focused in the junction area, making the effective junction area larger.

On the other hand, we know that superconductivity will be induced on the TI surface by proximity effect, spreading away to a distance of micron (Qu, F. et al., Sci. Rep. 2, 339 (2012); Yang, F. et al., Phys. Rev. B 86, 134504 (2012)). Therefore, the TI surface near Pb electrodes will be able to carry stray supercurrents.

After taking into consideration of the above facts, we employed an empirical method of estimating the effective junction area as shown in the right panel of Fig. S5. By comparing with the effective area drawn from the Fraunhofer pattern measurements, the effective area estimated by this method turns out to be accurate, with an error less than 20%.

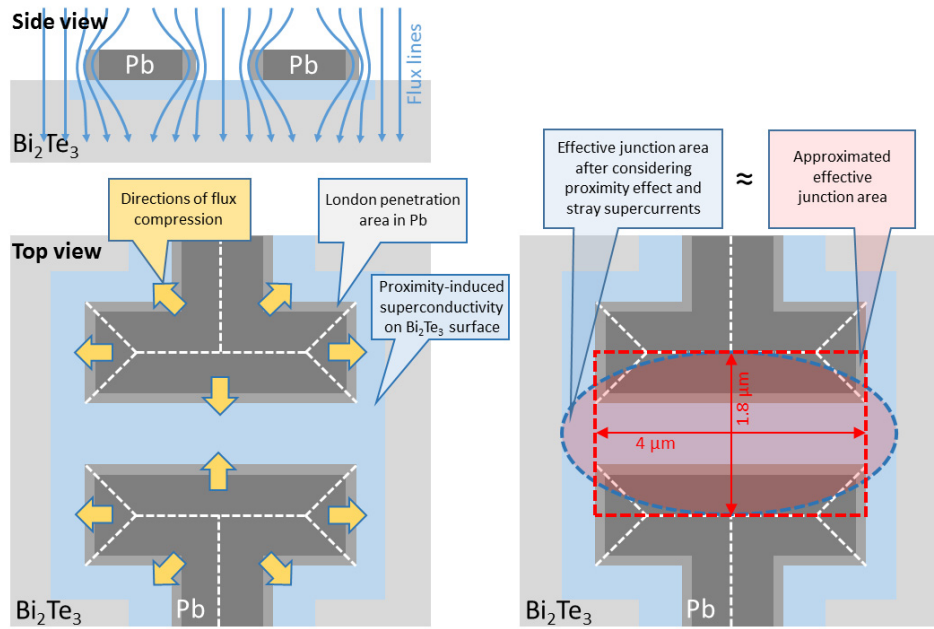


FIG. S5 | Upper left panel: Side view for flux compression. **Lower left panel:** Top view for flux compression. The flux in each area defined by white dashed lines will be compressed away along the arrowed directions. **Right panel:** Our empirical method of estimating the effective junction area after considering flux compression and stray supercurrent distribution.

